Global modes of ENSO and non-ENSO sea surface temperature variability and their associations with climate

DAVID B. ENFIELD

Atlantic Oceanographic and Meteorological Laboratory, NOAA
4301 Rickenbacker Causeway, Miami, Florida 33149 U.S.A.

ALBERTO M. MESTAS-NUÑEZ

Cooperative Institute for Marine and Atmospheric Studies
Rosenstiel School of Marine and Atmospheric Sciences, University of Miami
Miami, Florida 33149 U.S.A.

Abstract

In this chapter we review much of the recent work by others regarding the nature of the global modes of sea surface temperature (SST) variability and the SST involvement in interannual to multidecadal climate variability. We also perform our own analysis of global SST so as to describe the SST variability associated with El Niño/Southern Oscillation (ENSO) and the low-frequency modes not associated with ENSO (non-ENSO). ENSO is a global phenomenon with significant phase propagation between basins, which we preserve and describe using complex multivariate analysis, and subsequently remove from the global SST data. A similar analysis of the residuals reveals three non-ENSO modes of low-frequency variability related to signals described in the reviewed literature: (1) a secular trend representing the global warming signal with associated superimposed decadal variability; (2) an interdecadal mode with maximal realization in the extratropical North Pacific; and (3) a multidecadal mode with maximal realization in the extratropical North Atlantic. Relationships between SST and precipitation are analyzed with regression and multivariate analyses. These analyses show for the interannual-to-decadal time scales of the Western Hemisphere tropics that tropical Atlantic SST is comparable to the Pacific ENSO in its relevance to regional rainfall and is not redundant with respect to ENSO. Moreover, non-ENSO variability explains a significant fraction of the total cross-covariance between the two variables, and out-of-phase relationships between Pacific and tropical North Atlantic SST anomalies are associated with very strong rainfall departures over Central America and the Caribbean. We are led to conclude that present operational climate predictions can be significantly improved by extending numerical SST predictions from the Pacific to the world ocean and by enabling these models to emulate the observed non-ENSO modes of global variability.

Introduction

A great deal of research has been done on the Pacific El Niño/Southern Oscillation (ENSO) (see general reviews by Enfield 1989 and Philander 1990) and its climatic impacts (e.g., Ropelewski and Halpert 1987, 1989). ENSO is without a doubt the strongest, most globally coherent climate signal that exists in both the ocean and the atmosphere. Coupled ocean-atmosphere models developed in the past 15 years have demonstrated the potential for prediction of ENSO-related Pacific sea surface temperature (SST) fluctuations (Barnston et al. 1994). However, the numerical prediction of anomalous SST (SSTA) variability in other oceans—and their impact upon precipitation, in general—is not yet within reach and may require at least another decade of research. To get beyond the mere prediction of equatorial Pacific "warm events," value-added forecasts of land precipitation based on global numerical SSTA predictions and the empirical relationships between rainfall and SSTA must become a future norm.

One of the most attractive ways to mine the untapped predictability in the ocean-atmosphere system is to predict SSTA in other ocean basins at useful lead times of one to several seasons. Most, but not all, of this additional SSTA variability is not related to ENSO, is less well understood, and is presently unpredictable with operational methods. In this chapter we briefly review what is known about this added dimension of SST variability and its associations with rainfall in the Western Hemisphere. In addition, we will present new analysis of more than a century of global SSTA, its ENSO and non-ENSO components, and their relationships to previous knowledge of climate variability. To do this, SSTA will be separated into a global, propagating ENSO component, and the statistical modes of the non-ENSO residuals after removal of the ENSO component. We will describe the nature of both components and will show that the ways in which the Pacific and Atlantic SSTA combined are of fundamental importance to the nature of precipitation anomalies in the tropical Americas.

Non-ENSO variability: A review

It has been amply demonstrated that non-Pacific modes of SSTA are related to land climate, especially rainfall. Folland et al. (1986) showed that meridionally antisymmetric contrasts in global SSTA between the Northern and Southern Hemisphere have a significant influence on rainfall over the African Sahel. The many other studies of Atlantic SST and Northwest African rainfall include Citeau et al. (1989) and Lamb and Peppler (1992), who show how the linkage works through the effects of meridional gradients in SSTA on the meridional position of the intertropical convergence zone (ITCZ, where the northern and southern trade wind regimes converge and convective activity and rainfall are large; see also Wagner 1996). More than a decade of research by Hastenrath and colleagues has documented the combined effects of eastern Pacific (mostly ENSO) and tropical Atlantic SSTA on inter-American rainfall (Hastenrath 1978, 1984; Hastenrath et al. 1987; Hastenrath and Greischar 1993). A number of studies have demonstrated the powerful effects of tropical Atlantic SSTA—especially its meridionally antisymmetric component—on the rainfall in Northeast Brazil (e.g., Moura and Shukla 1981; Nobre and Shukla 1996).

The above studies mainly document relationships between SSTA and rainfall in the near-equatorial tropics. As with ENSO, however, Atlantic SST variability can affect rainfall at higher latitudes as well. Enfield (1996) shows that tropical North Atlantic SSTA has an effect on rainfall

comparable to that of the Pacific ENSO throughout the Intra-American Sea (IAS) and surrounding land regions from northern South America to the southern United States (Fig. 1).

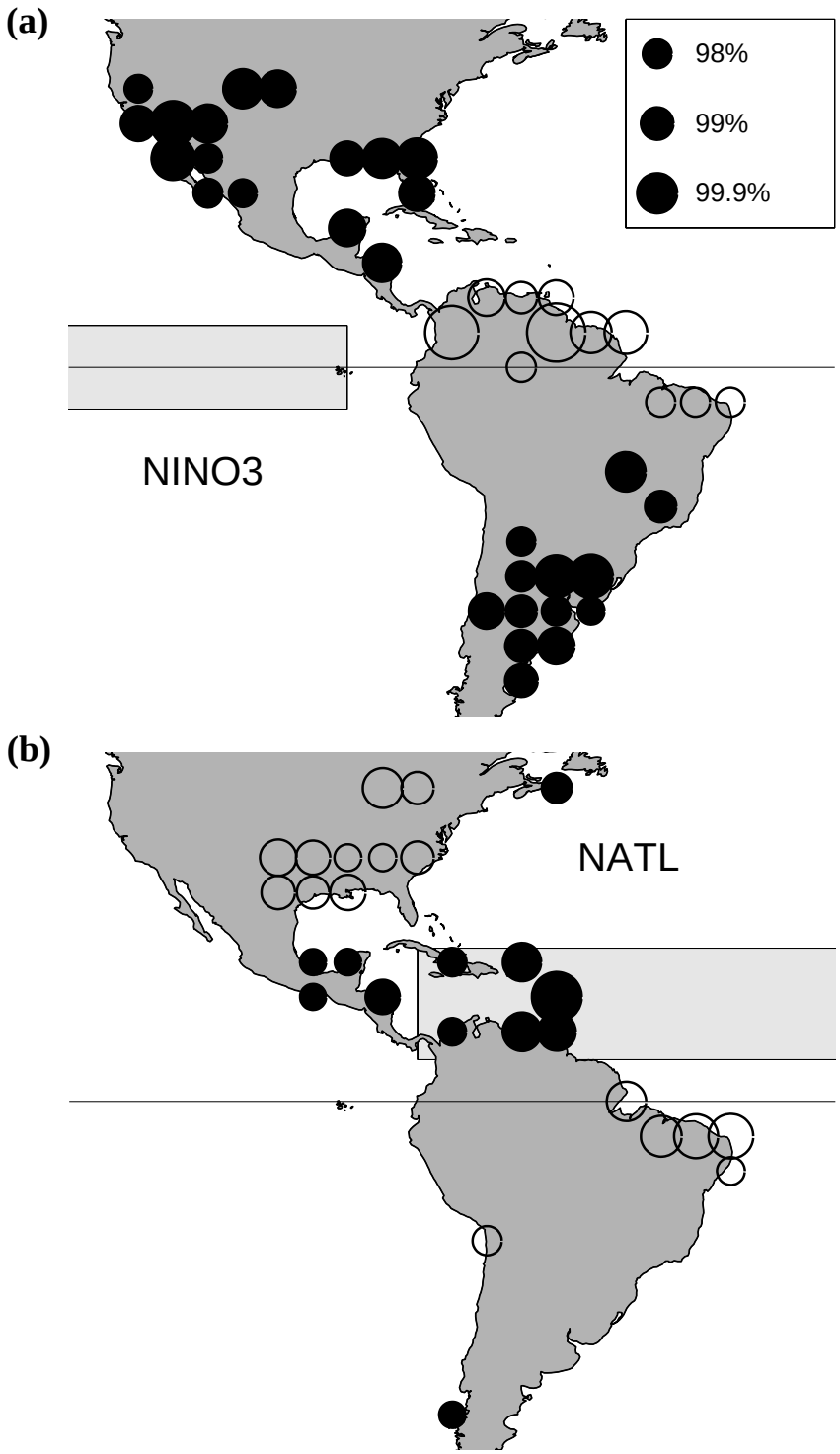

Fig. 1 Relative magnitudes (circle diameters) and sign (solid positive, unfilled negative) of maximum lagged (0–3 seasons) correlations between U.S. Department of Energy 5- by 5-degree gridded rainfall departures and the NINO3 (a) and NATL (b) indices of sea surface temperature anomaly variability, defined as simple averages over the regions ±6°, 90°–150°W and 6°–22°N, 15°–80°W, respectively. The inset legend shows the circle diameters corresponding to several significance levels (serial correlation accounted for). The very small dots show grid points where data exist.

While noting that equatorial Pacific and tropical Atlantic SSTA are intercorrelated through the extension of the Pacific ENSO signal into the Atlantic (Enfield and Mayer 1997), Enfield (1996) observes that the Atlantic SSTA-rainfall correlations over the IAS region are mostly of the wrong sign to be explained by the intercorrelation of SSTA between basins. Apparently, the tropical Atlantic has non-ENSO seasonal-to-interannual SST variability related to climate, but the Atlantic extension of the ENSO SST signal through tropospheric forcing (Hameed et al. 1993; Enfield and Mayer 1997) tends to mask and complicate interpretation of the Atlantic-only processes that may exist. The correlation between equatorial Pacific SSTA and large-scale averages of tropical North Atlantic SSTA is about 0.5, hence about three-fourths of the Atlantic variability is non-ENSO in nature. The global distribution of the Pacific ENSO SST signal is a problem for the detection and attribution of non-ENSO SST-climate relationships, and preferably should be accounted for prior to further analysis.

One such Atlantic-only relationship is the tendency noted by some for the tropical North Atlantic (5°–25°N) and South Atlantic (0°–20°S) SSTA regions to correlate antisymmetrically across the ITCZ in what is sometimes referred to as the tropical Atlantic dipole (Weare 1977; Servain 1991), and for such covariability to be strongly related to rainfall anomalies in Northwest Africa and Northeast Brazil (e.g., Moura and Shukla 1981; Nobre and Shukla 1996). However, statistically significant dipole variability is difficult to detect at seasonal-to-interannual time scales (Houghton and Tourre 1992; Enfield and Mayer 1997) perhaps due to the masking influence of the extended ENSO signal, which is not antisymmetric in nature (Enfield and Mayer 1997).

The tropical Atlantic dipole is but one aspect of Atlantic variability from Antarctica to Greenland. Both observations and models indicate that the interannual variability associated with the tropical North Atlantic extends to the high northern latitudes in the form of broad, co-oscillating zonal bands of alternating phase, and with enhanced variance in the western portions off North America (e.g., Delworth 1996). North of the tropical North Atlantic lies an anticorrelated band, in the range of 30°–45°N, followed by an in-phase band south of Greenland (45°–65°N), while to the south of the tropical South Atlantic lies another in-phase band.

It appears that the primary cause of interannual SSTA variations at non-equatorial latitudes is through thermodynamical air-sea fluxes across the sea surface and not through ocean dynamics (Delworth 1996; Enfield and Mayer 1997). The anomalous fluxes are associated with wind fluctuations that are in turn a consequence of anomalous tropospheric circulation patterns such as the Pacific North American (PNA) and North Atlantic Oscillation (NAO). These are two of the more significant “teleconnection patterns” in tropospheric pressure fields, which have been documented by Barnston and Livezey (1987), Wallace et al. (1990), and others. The PNA pattern is the one associated with ENSO variability; it has its strongest node over the North Pacific, associated with fluctuations in the Pacific subtropical jet stream and with ENSO-related climate anomalies over the continental United States. The NAO has a strong node over Greenland and an antinode over the subtropical North Atlantic, and is associated with fluctuations in the North Atlantic westerly winds and with climate over central and northern Europe (Hurrell 1995). The PNA and NAO pressure patterns are both associated with Atlantic subtropical pressure fluctuations, which in turn affect the strength of the low-latitude North Atlantic trade winds. The ENSO-related PNA fluctuations are the most likely explanation for the extension of ENSO variability into the tropical North Atlantic SSTA, as noted by Enfield and Mayer (1997).

An important dimension to non-ENSO variability is its existence at decadal and longer time scales in both the Pacific and Atlantic. The tropical Atlantic dipole is possibly one example of this. While not ubiquitous at the ENSO seasonal-to-interannual time scale, the dipole emerges more

clearly at longer, 10–20 year periodicities (e.g., Carton and Huang 1994; Mehta and Delworth 1995; Huang et al. 1995; Chang et al. 1997). Because these interdecadal variations affect the ITCZ and are associated with extended droughts in Northeast Brazil and Northwest Africa, there is a great need to improve our understanding of them.

Another example of interdecadal variability (from observations) is found in a Pacific SSTA mode, linearly independent of ENSO (Deser and Blackmon 1995; Latif and Barnett 1996). It has a strong nodal region centered along 40°N and west of 140°W, and a co-oscillating companion region east of Australia. From 1949 through the early 1990s, the 40°N nodal region oscillated between multiyear warm periods and cool periods. Simultaneously, the tropical Pacific (±20) and the high latitudes off the west coasts of North and South America underwent shifts of opposite sign. A number of ocean-atmosphere interactive mechanisms have been proposed (using models) to account for this cyclicity (e.g., Latif and Barnett 1994; Gu and Philander 1997). The spatial pattern of the mode bears a certain resemblance to the ENSO SSTA pattern, but how they are related, or whether one merely provides a slowly varying background for the other, is not understood.

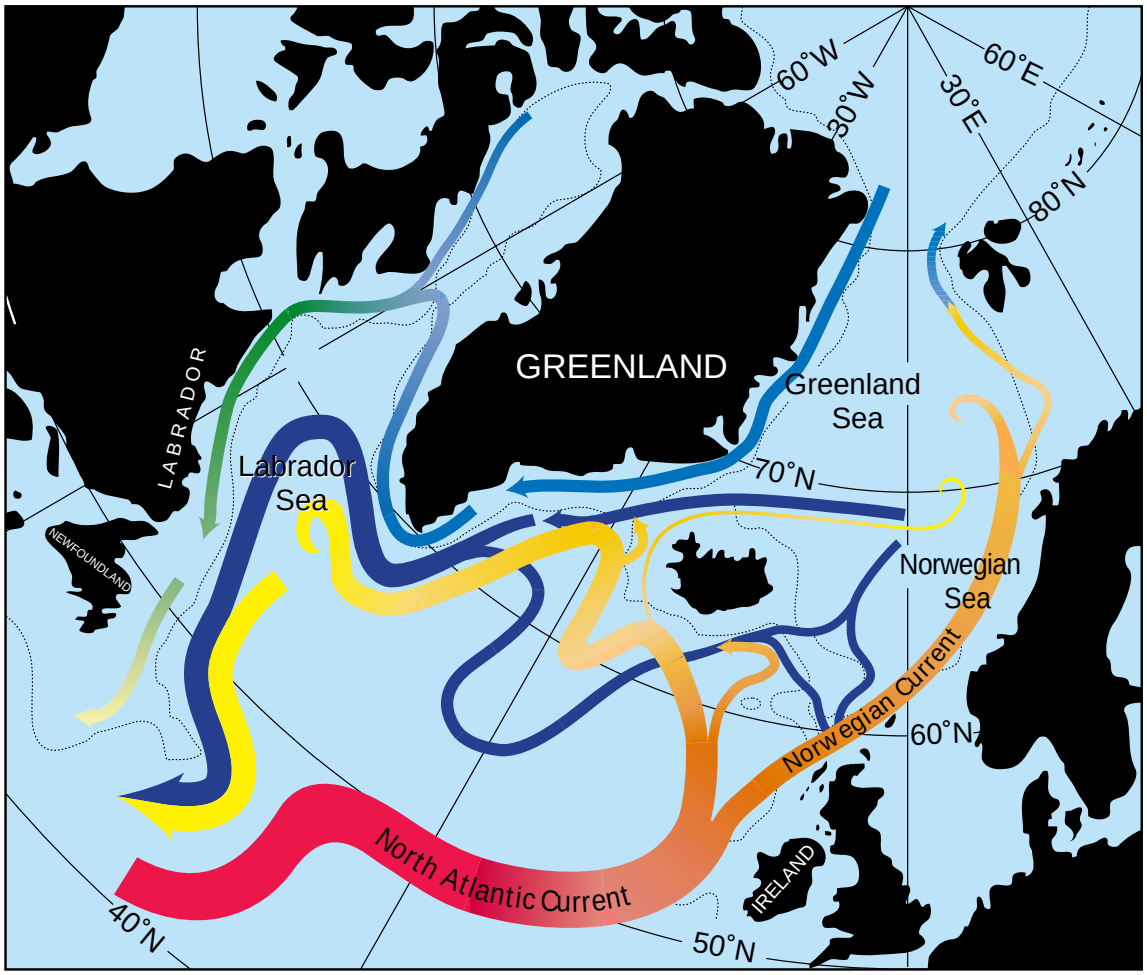

Fig. 2 Schematic illustration of the pathways associated with the advection and transformation of subtropical and subpolar surface water masses, wherein sea surface temperature anomalies eventually modify newly formed deep water through subduction, to complete a long-term climate cycle. The figure is a reproduction from McCartney et al. (1996), who describe this mechanism to explain the multidecadal climate variability.

A longer, multidecadal cycle exists in the Atlantic SSTA north of about 30°N, which involves cool temperatures prior to about 1940, warm conditions during 1951–67, and cool conditions again during 1968–77 (Kushnir 1994; Hansen and Bezdek 1996). This oscillation coincides with a similar long-period fluctuation in the North Atlantic sea level pressure (SLP) field and midlatitude zonal winds (Kushnir 1994) and in the NAO index (McCartney et al. 1996; Hurrell 1995). It also agrees with the North Atlantic SSTA variability seen in the third rotated empirical orthogonal function (EOF) mode of Kawamura (1994). These features may be related through ocean-atmosphere interactions involving a waxing and waning of the mid-North Atlantic westerly winds, slow advection of SST anomalies around the subtropical and subpolar gyres, and subduction of SSTA to greater depths in the Labrador Sea (McCartney et al. 1996; Curry and McCartney 1996). The water mass pathways for this hypothesized mechanism are shown schematically in Figure 2. The primary climatic impact of the oscillation derives from its association with alternating, multiyear periods of mild and severe winters in central Europe and the Mediterranean Sea (McCartney et al. 1996; Kerr 1997).

The global ENSO in SST

Before we can explore what is *not* ENSO in global SSTA, we must first define the ENSO SSTA signature, compute it, and describe it. Once a reasonable space-time representation is obtained, we will subtract it from the data and examine the residuals. We must use a global data set so as not to limit ENSO to the tropical Pacific, because tropospherically connected ENSO signals elsewhere in the world ocean (Covey and Hastenrath 1978; Hastenrath et al. 1987; Latif and Barnett 1995; Tourre and White 1995; Lanzante 1996; Enfield and Mayer 1997) also affect the global climate (Lau and Nath 1994). We also require a century-scale data set to detect secular trends and resolve decadal to multidecadal fluctuations.

The 1856–1991 reconstruction of historical ship-based data by Kaplan et al. (1998, henceforth K) is ideally suited for this purpose. The K analysis uses the covariance structure of the global SST anomaly field to fill missing data in a statistically optimal way, and reconstructs the data based on the first 80 empirical modes of the modern portion of the data record in a manner analogous to that of Smith et al. (1996). Such reconstructions are not well suited to analysis on small regional scales, because they smooth out the variability at high frequencies and small space scales. However, for the basinwide scales typical of ENSO and interdecadal variability, they pose special advantages, especially for early periods that were more sparsely sampled than the modern era.

The K data are first smoothed with a low-pass filter that eliminates periodicities of 1.5 years or less. These smaller time scales include intraseasonal and month-to-month variations associated with the smaller regional space scales for which the reconstructed data are less appropriate. For the calculation of the global ENSO component we apply an additional, high-pass filter to temporarily remove periodicities longer than 8 years, yielding a 1.5- to 8-year band-pass for the ENSO component. When the ENSO component is subsequently removed from the smoothed K data, the residuals contain non-ENSO variability at all periodicities longer than 1.5 years. Trends are not eliminated, because they are associated with secular variations that are probably real and correspond to observed global warming. They are removed from the ENSO analysis by the 8-year filter but reappear in the residual (non-ENSO) variability and are captured in one of the non-ENSO modes.

EOF analysis, also known as principal component analysis (PCA), consistently extracts from SSTA data a dominant ENSO-related mode as a first or second component. See, for example, the first rotated EOF of Kawamura (1994). Hence, one approach for defining and removing the global ENSO is to compute the EOFs of the band-passed global SSTA and subtract the first-mode data reconstruction from the original data. A similar approach was adopted by Cane et al. (1997) to isolate century-scale trends from the effects of low-frequency changes in ENSO behavior. However, while the dominant mode of Pacific variability associated with ENSO appears quasi-stationary (in or out of phase), meridional phase propagation of SSTA occurs over a significant region offshore of the eastern Pacific boundary, while other research indicates that tropospherically connected phase propagations to other ocean basins also exist (e.g., Latif and Barnett 1995). Ordinary EOF analysis misrepresents such propagations, and the quadrature component of variability associated with them will not be included in the dominant mode. Hence it will not be removed and will "contaminate" the residual data. Because we are especially interested in the non-ENSO variability found in other ocean basins, a modified analysis (without this drawback) must be applied.

To account for the phase propagations, we perform a standard eigenvector decomposition on a transformed, complex data set that comprises the bandpassed K data (real part) and its Hilbert transform (imaginary part). The standard EOF procedure applied to the complex data then yields a complex EOF result (CEOF) in which spatial and temporal phase information is preserved in the ENSO-related first mode (Rasmusson et al. 1981). Lanzante (1996) used a very similar approach to analyze the amplitude and phase structure of the ENSO mode in the global tropics for the 1875–1979 time period, but without first eliminating decadal and longer time scales.

The spatial amplitude, spatial phase, and temporal realization of the first global CEOF mode are shown in Figures 3a, 4a, and 5a, respectively. The mode explains 34.4% of the global variance in the band-passed data and 17% of the low-passed K data. The local explained variance in the regions of high (low) amplitudes (Fig. 3a) are of course much larger (smaller) than the global amount. In the discussions of Figure 3 that follow, spatial amplitudes occurring in the upper half of the color palette denote regions of high, or primary, loading (importance to the mode), blue colors denote intermediate, or secondary, loading, and magenta denotes low, possibly insignificant, loading.

Here (as also in the non-ENSO modes) we choose a rectangular index region—not too large—where spatial amplitude is large and spatial phase is fairly uniform, to serve as a reference for the temporal variability. The obvious reference rectangle for the ENSO mode is the well-known NINO3 region in the equatorial Pacific, bounded by 5°N–5°S, 90°W–150°W. In Figure 5a we show the temporal realization (temperature units) for phases and amplitudes combined over NINO3 rather than the more confusing temporal amplitude and phase functions from which they are derived (i.e., the complex expansion coefficients for the mode). The time variability elsewhere is merely the same series lagged by the appropriate spatial phase (Fig. 4a) and with amplitude scaled in proportion to the spatial amplitude (Fig. 3a). The color palette for the spatial phase (Fig. 4a) has been rotated so that the average spatial phase over the NINO3 region corresponds to ±180 degrees (red), and a zero lag (months, contours). There are 37 zero upcrossings in the 135-year NINO3 series (Fig. 5a), yielding an average period of 43.7 months. This is about midway in the 3- to 4-year range usually attributed to ENSO variability and corresponds to 8 degrees of spatial phase per month of lag.

Our treatment of the time realization requires further explanation. It may be unfamiliar to specialists accustomed to seeing temporal amplitude and phase functions, but the latter would be

difficult to interpret for the nonspecialist. One must understand that Figure 5a is not an average of the data over the NINO3 region. Rather, it is the average over the NINO3 region of the SSTA reconstructed from the ENSO mode. It is therefore the ENSO mode contribution to the data-based version of NINO3 and as such has some differences with respect to the latter. Notice, for example, that the 1982–83 warm event (El Niño) is not the strongest ENSO fluctuation in the record, as a similarly filtered average of the SSTA data would show. That is because part of that event's amplitude is actually in the slowly varying background state which was warm during the 1980s. That background condition is captured by the slower non-ENSO modes discussed in the next section.

The spatial functions (Figs. 3a, 4a) show the classical features normally associated with ENSO in the Pacific: (1) a region of intense amplitude within ±5°–10° of the equator and east of the date line, decreasing to smaller amplitudes over a wide, wedge-shaped region that spreads poleward along the eastern boundary; (2) phase propagation northward along the coast of North America, with maximum lags of one to two seasons in the Gulf of Alaska and Bering Sea; and (3) regions of intermediate amplitude and opposite phase in the central North Pacific (30°–45°N), the western South Pacific (20°–40°S), and the tropical western Pacific. Less documented features include one-season lags in the central Pacific near ±20°; and a precursor off central Chile with a one-season lead. Although a large region of the Southeast Pacific has few data (unshaded area, offshore), the latter feature lies along the coastal ship route north of Cape Horn that has been relatively well sampled since the nineteenth century, and the precursor has been previously mentioned by Rasmusson and Carpenter (1982). A possible cause of the precursor is a weakening in the southeast trades (and associated surface heat fluxes) off Chile, prior to the main trade wind weakening at lower latitudes.

Both the tropical Atlantic and Indian Oceans show known coherence and lag structures relative to the equatorial Pacific. The tropical Atlantic is lagged by 3–9 months with a phase propagation from higher to lower latitudes. Regions of maximum amplitude occur near ±20° with a two-season lag, consistent with the results of Enfield and Mayer (1997). The Indian Ocean is similarly lagged with eastward phase propagation, consistent with Latif and Barnett (1995). Very little coherent variability is found in the North Atlantic, north of 20°–30°N. The lack of coherent variability off Angola (0°–20°S) and the somewhat larger lags in the western equatorial Atlantic are qualitatively consistent with the structures found by Enfield and Mayer (1997).

The above characteristics of the global ENSO are consistent with the similar but more detailed analysis of Lanzante (1996). Although Lanzante does not discuss this, his breakdown of the 1875–1979 data period into three shorter periods shows that the larger lags in the equatorial Atlantic existed only during 1950–79 and not during the previous 75 years. His tropical Atlantic lags are quite uniform during the earlier periods and are similar to the modern lags in the 5°–15°N band. It is not clear whether the meridional lag structure in the Atlantic (Fig. 4a) is a nonrobust feature of the system, or one that is more ubiquitous but poorly captured under the sparser sampling of the earlier periods.

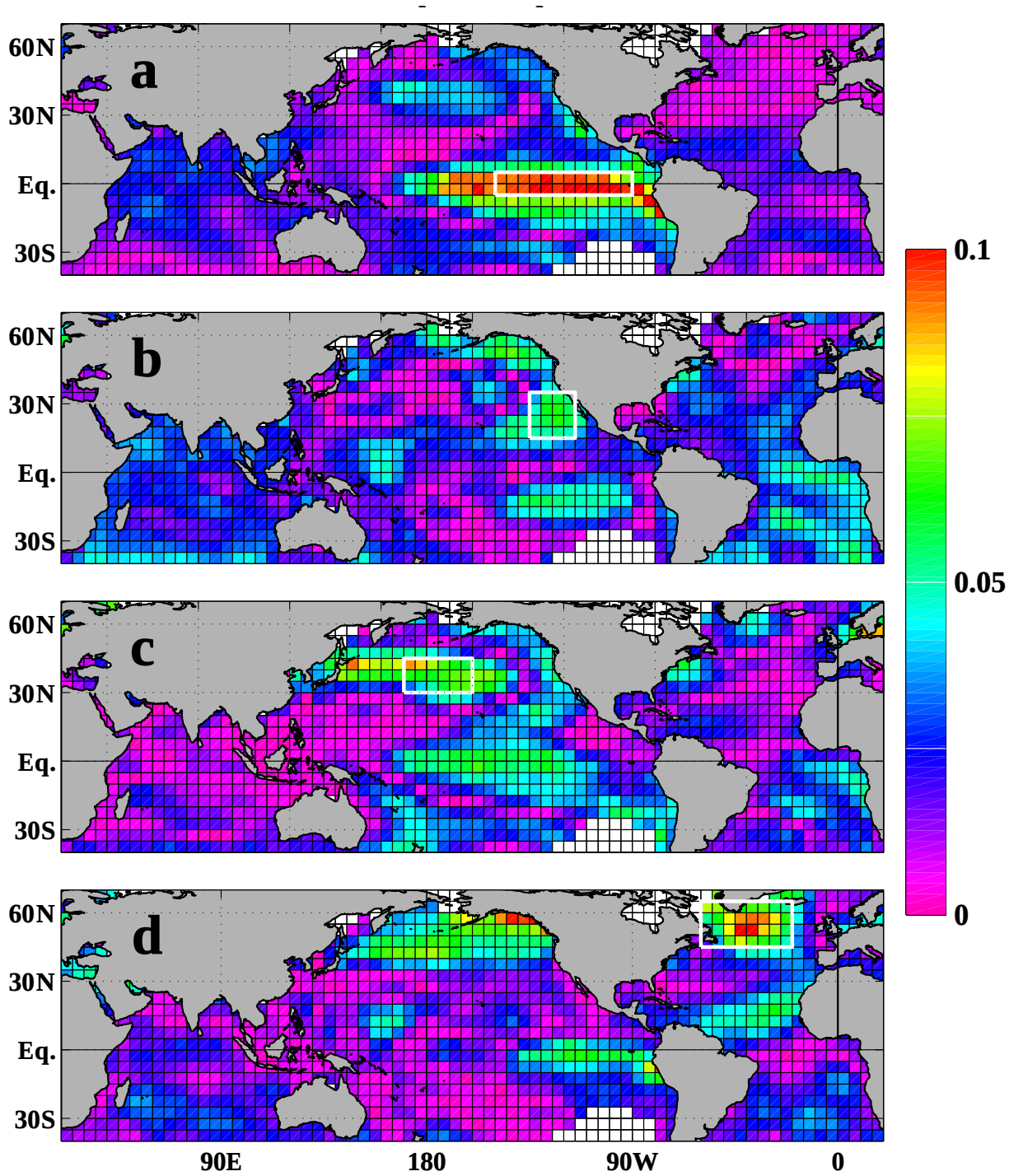

Fig. 3 Distributions of spatial amplitudes for the first complex empirical orthogonal function (CEOF) eigenvector describing global ENSO variability (a), and for the first three CEOF eigenvectors describing non-ENSO variability (b, c, d), as discussed in the text. The white rectangles on the maps outline areas of high amplitude discussed in the text and used to form the temporal realizations (Fig. 5).

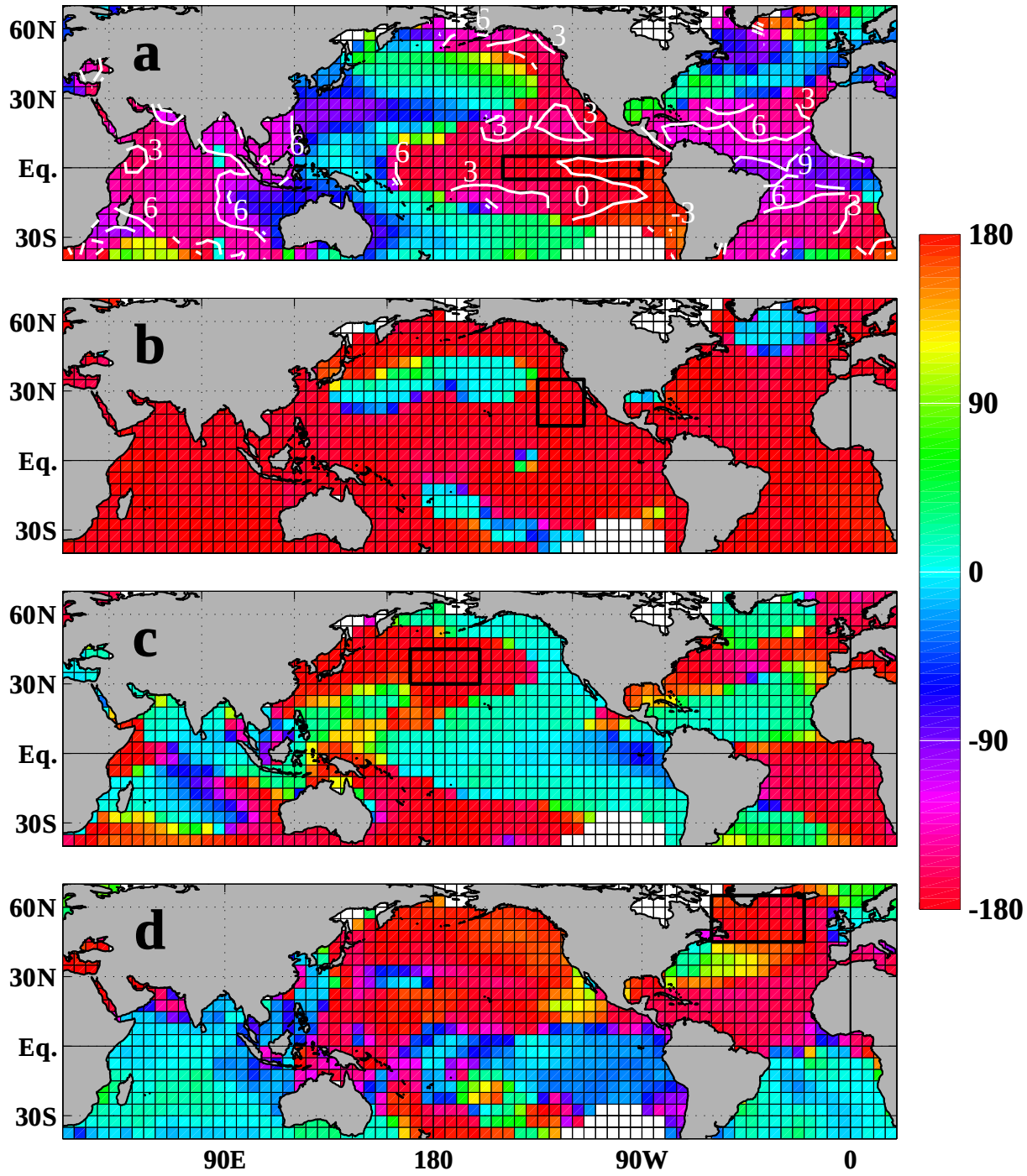

Fig. 4 Distributions of spatial phases (degrees) for the first complex empirical orthogonal function (CEOF) eigenvector describing global ENSO variability (a), and for the first three CEOF eigenvectors describing non-ENSO variability (b, c, d), as discussed in the text. The black rectangles on the maps outline areas for which the spatial phase is referenced to $\pm 180^{\circ}$. Phase advances in the direction of higher values. Lag contours are shown in the ENSO distribution (a) for lags of -3, 3, 6, and 9 months relative to the average phase for the NINO3 region.

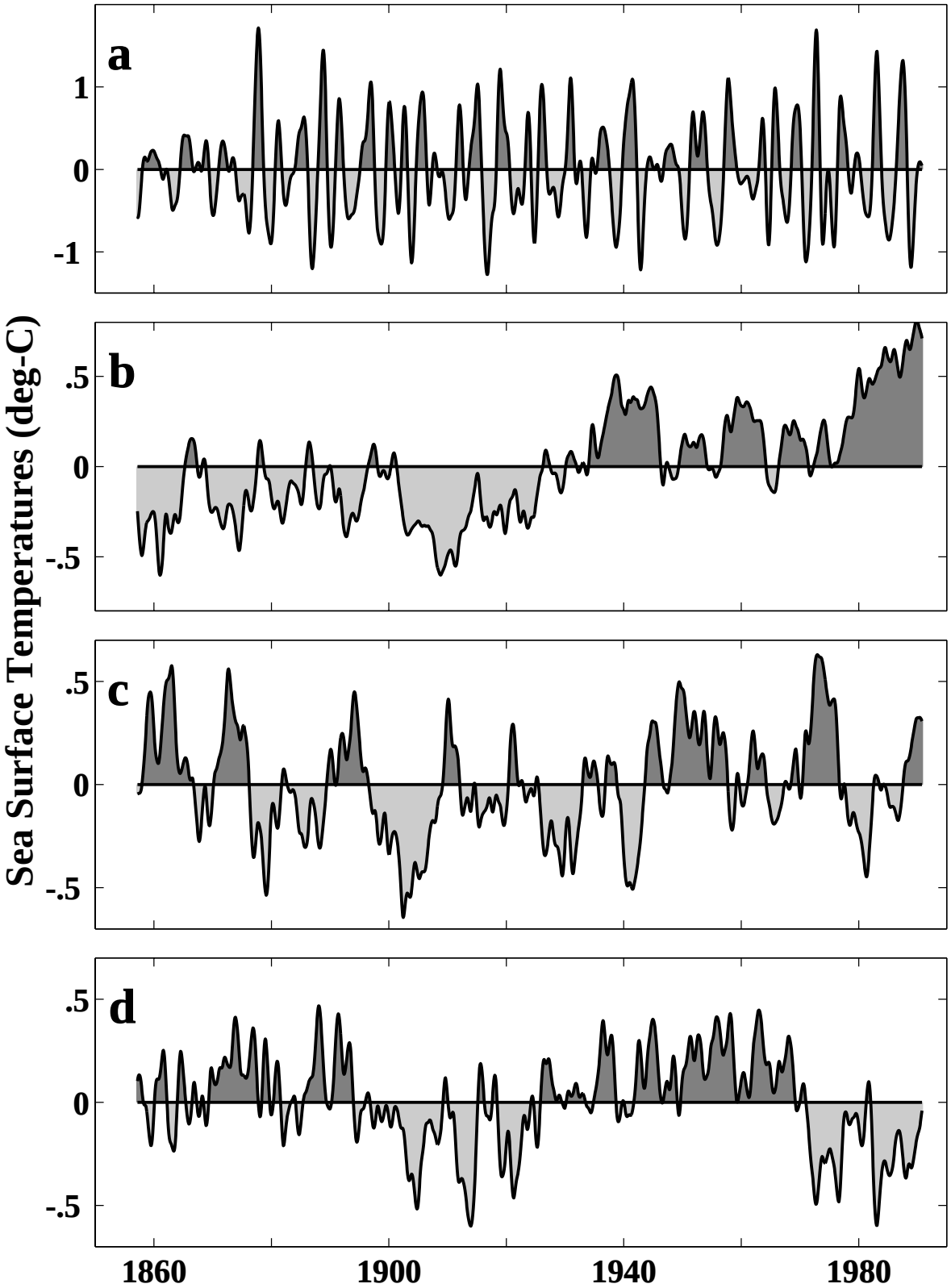

Fig. 5 Temporal realizations for each of the complex empirical orthogonal function (CEOF) modes in Figures 3 and 4, computed by averaging the modal reconstructions over the respective rectangular regions shown in the spatial distributions.

The non-ENSO SST variability

To form a non-ENSO global data set, the SSTA reconstruction from the leading CEOF in the ENSO band (Figs. 3a, 4a, 5a) was subtracted from the low-passed (1.5-year) K data, and the CEOF modes were recalculated. The first three CEOF modes account for 16%, 9%, and 7% of the variance in the non-ENSO residuals and 15%, 8%, and 5% of the low-passed K data (before removal of ENSO). The latter amounts can be compared with the 17% explained by the ENSO component. The spatial amplitudes, spatial phases, and temporal realizations for the first three non-ENSO modes (panels b, c, d) are shown in Figures 3, 4, and 5, respectively. The rectangular box shown in each spatial pattern is a region of large spatial amplitude (Fig. 3) and uniform spatial phase (Fig. 4) to which each temporal mode realization (expansion coefficients) was referenced. In the case of modes 2 and 3, the boxes overlap with key regions discussed by others and referred to in the review section.

All of the spatial patterns correspond to quasi-stationary oscillations wherein significantly loaded antipodal regions are 180° out of phase with respect to each other and propagating phases are infrequent. The areas of low loading frequently occur in regions of rapid phase change between spatial antipodes, as we would expect of a stationary oscillation. Also as expected of stationary oscillations, very similar patterns emerge from an ordinary EOF analysis of the low-passed data (not shown). As a check on the robustness of the modes to filtering, the CEOF procedure was also applied to both the raw (unfiltered) non-ENSO residuals and very low-pass (8-year cutoff) K data. In both cases, all three of the residual modes shown emerged within the first four modes. Only in the case of the unfiltered data, a mode dominated by very high frequencies was promoted with respect to mode 3 of this analysis, while modes 1 and 2 always occurred as before.

Mode #1: Global warming

It is clear from the temporal realization of mode 1 (Fig. 5b) that this mode contains the global warming signal. Comparison with Jones et al. (1986) and Houghton et al. (1996) confirms that this signal is the ocean counterpart to the global warming seen in surface air temperatures. Areas of significant loading (Fig. 3b) are as extensive as in the global ENSO mode. The dominance of red colors in the spatial phase (Fig. 4b) shows that warming occurs almost everywhere except for secondary cooling in the midlatitudes of the central and western North Pacific. More intense warming occurs in the Gulf of Alaska and in the core regions of the trade wind belts, especially in the east-central parts of the Pacific and South Atlantic. In his rotated EOF analysis of SSTA, Kawamura (1994) appears to have captured parts of our global warming mode in his second (Pacific and Indian Oceans) and fourth (South Atlantic) modes.

The least-squares-fitted linear trend to Figure 5b is 0.55°C per century, as compared with 0.22°C per century for the trend in the globally averaged SST (not shown). The difference reflects the greater degree of increase in the regions of primary warming (Fig. 5 is indexed to the box regions in the spatial distributions). After 1900, the trends are 0.93°C and 0.42°C per century, respectively, while prior to 1900 the warming is negligible. The residuals about the trend show significantly higher spectral energy at periodicities of 1–2 decades, also seen in the globally averaged data, and the oscillations are also larger in the regions of high loading than globally.

Mode #2: Pacific interdecadal

Mode 2 is dominated by the central and eastern Pacific and has little significance in the Indian or western tropical Pacific Oceans. Warmings in the central North Pacific reference region are in phase with energetic fluctuations along an extensive midlatitude zonal band (30°–50°N) stretching from Japan to about 140°W. Another area of in-phase variability is found south of 10°S and east of Australia, near the date line. Antipodal variability, out of phase with the reference region, is strongest along the equator in the central Pacific and extends poleward and eastward over a large triangular region of the Tropics and along the extratropical Pacific coasts of North and South America. The Atlantic in-phase regions are the east-central portion of the tropical South Atlantic and the Northwest North Atlantic region bounded by North America, the Gulf Stream extension, and the 55°W meridian. Atlantic antipodal variability occurs southeast of Greenland and to a lesser degree in the eastern Caribbean and east of southern Brazil near 20°W.

This pattern is coherent with the distribution of correlation between SST observations and a North Pacific SST index bounded by 25°–40°N, 170°E–160°W (Latif and Barnett 1996). The differences in the spatial distributions are very minor and can probably be explained by the much shorter time period (1949–92) used by Latif and Barnett. The extended time series for their index, calculated from the low-pass-filtered (1.5-year) K data, has a correlation of 0.65 with our mode 2 realization. Thus, mode 2 efficiently captures the Pacific interdecadal mode discussed in the review section.

Mode #3: Atlantic multidecadal

The third mode is dominated by two realizations of a 70- to 80-year cycle with weaker, interannual variability superimposed (Fig. 5d). Its spatial amplitude is largest in the far North Atlantic southeast of Greenland and north of the Gulf Stream extension (Fig. 3d). The mode is also strong north of 40°N in the North Pacific and has secondary regions of moderately strong activity in the eastern equatorial Pacific and the tropical North Atlantic. Significant variability also occurs in the Indian Ocean and the South Atlantic. Especially interesting is the alternation of phase between the Northern and Southern Hemispheres (Fig. 4d).

In more respects than not, this mode corresponds to the second EOF of global SSTA (1949–92) computed by Nicholls et al. (1996), including its strength in the North Atlantic, the southern Indian and Atlantic Oceans, and the east-central equatorial Pacific, as well as in the alternation of phase between the Northern and Southern Hemispheres. The polarity shift (circa 1965–70) noted by Nicholls et al., from a cold to a warm (warm to a cold) background condition in the Southern (Northern) Hemisphere, is also reproduced in the temporal realization (Fig. 5d), but is now seen to be an alternating transition that occurs at roughly 35- to 40-year intervals. The temporal variation also corresponds to a similar cycle of warming and cooling noted by others for the western extratropical North Atlantic (Kushnir 1994; Hansen and Bezdek 1996; McCartney et al. 1996). These variations are known to have a strong association with tropospheric pressure fields (Kushnir 1994), wind strength in the midlatitude westerlies (Deser and Blackmon 1993), and the NAO (Hurrell 1995; McCartney et al. 1996). While the focus of ocean-atmosphere interaction appears to be in the Atlantic sector, its ramifications are clearly global in scope.

Relationships between SSTA and rainfall

Difficulties with rainfall data have been an impediment to understanding the SST-rainfall relationships at the decadal to multidecadal time scales shown in the non-ENSO SST modes. Reliable rain gauge records of a century or more that can resolve these longer time scales are scarce, are difficult to obtain, or present special challenges due to changes associated with instrumentation, station location, and land use practices. However, the potential for the low-frequency changes in SST to influence climate can be seen in the many analyses of the joint variability of SSTA and tropospheric pressure and wind fields (e.g., Wallace et al. 1990; Deser and Blackmon 1993; Kushnir 1994; Trenberth and Hurrell 1994). It is possible that the ocean plays the role of a pacemaker, introducing persistence into the tropospheric variations, which in turn can condition longer term variations in rainfall. In this section we will recap other research regarding the relationships of rainfall at the long time scales to our non-ENSO modes of SST variability. In the following section we also present new analyses that illustrate certain principles as they apply to the interannual-decadal time scale.

Comprehension of global trends in rainfall and their attribution to the global warming mode (Figs. 3b, 4b, 5b) are elusive at best and benefit from ancillary analysis, such as through modeling, to achieve added plausibility. Even where usable long rainfall records exist, the associations of secular changes in rainfall with possibly related SST trends, while common, have little or no statistical significance. Nevertheless, a few studies have documented precipitation effects more directly. Thus, when long rainfall records are averaged over land areas (post-1900), there is a small upward trend in rainfall globally of 1% and there are much larger areas of rainfall increase than of decrease (Houghton et al. 1996). According to Hurrell (1995), "the recent warming may be related to increasing tropical ocean temperatures that have led to an enhancement of the tropical hydrological cycle."

The Pacific interdecadal mode (Figs. 3c, 4c, 5c) appears to be related to precipitation over North America, downstream from the Pacific focus of the principal ocean-atmosphere interactions. Latif and Barnett (1996) have described an association between this mode and interdecadal climate oscillations over North America. Ting and Wang (1997) note two modes of influence on summer rainfall in the central United States. One, related to the tropical Pacific, is interannual and clearly involves ENSO. The other mode involves the extratropical North Pacific and exhibits interdecadal variability with a spatial distribution of SSTA that strongly resembles our second non-ENSO mode in the Pacific. When SSTA is positive in our central North Pacific index region, their analysis shows a decreased SST gradient south of there, reduced intensity in the overlying mid-Pacific jet stream, and increased precipitation downstream over the east-central United States (30°–40°N). Neither the winter precipitation nor the effects of Atlantic SSTA were considered in their study.

In analogous fashion, climate variability in Europe is related to North Atlantic SSTA, which in turn corresponds to our third mode of non-ENSO SSTA (Figs. 3d, 5d). The relationship begins with the observation that the ocean temperatures in and near the Labrador Sea (Fig. 3d, box area) are inversely related to the NAO and the strength of the midlatitude westerly winds (McCartney et al. 1996; Kerr 1997). During winters in which SST is low and the NAO is significantly stronger than normal, the North Atlantic westerlies strengthen and tilt along an axis directed more to the northeast, bringing more moisture to Scandinavia and leaving central Europe and the Mediterranean relatively dry (Hurrell 1995). The covariations of rainfall and SSTA occur on the slow time scale seen in Figure 5d, possibly conditioned by North Atlantic Ocean circulation and the formation of anomalous deep water in the Labrador Sea (McCartney et al. 1996; see Fig. 2).

Interactions between oceans

At present, operational climate predictions are based only on the prediction of ENSO-related SST in the Pacific. Neither the non-ENSO modes such as are discussed in this chapter, nor the Atlantic and Indian Ocean extensions of ENSO are considered. In this section we argue that predictions should be global and that non-ENSO variability should be included.

The advantage of implementing predictions globally may seem obvious. But, since each of the various modes of variability (ENSO and non-ENSO) appears to be weighted more strongly in one of the three oceans, one might ask whether SSTA needs to be predicted globally, as the modal extension into the other basins might be considered redundant. The numerical model experiments of Lau and Nath (1994) illustrate why this is not the case. In their experiments, a model atmosphere was alternately forced by observed SST in a global ocean (Global Ocean–Global Atmosphere, GOGA—tropics and extratropics, all basins), a tropical ocean (Tropical Ocean–Global Atmosphere, TOGA; tropical Pacific), and a Midlatitude Ocean–Global Atmosphere, (MOGA; extratropical Pacific). The outcomes were arbitrated by comparing the singular value decomposition (SVD) of SST and Northern Hemisphere 500 mb height for each model run against an SVD for global SST and Northern Hemisphere 500 mb data sets. Both GOGA and TOGA reproduced qualitatively the principal features in the data—both dominated by the known SST and 500 mb patterns associated with ENSO—while MOGA came in a poor third. However, only GOGA quantitatively approached the observations, while the 500 mb pattern intensity for TOGA was significantly less intense. The implication is that ENSO-related SST variability outside the tropical Pacific, though redundant in the time domain, reinforces the Pacific and results in a more realistic atmospheric pattern. Although only the first SVD mode was examined, dominated by ENSO and interannual variability, a similar principle presumably applies to the non-ENSO modes discussed in this chapter.

We might also inquire as to what extent signals in other basins can compete with the ENSO signal in climate, or add to ENSO-based predictability. This is not clear even if we choose alternative predictors in a non-Pacific basin, because the ENSO signal is global and therefore some degree of intercorrelation (involving ENSO) exists between basins, confounding the identification of other relationships. For example, both the NINO3 and tropical North Atlantic (NATL, see Fig. 1) have comparable rainfall correlation patterns over much of the Americas. But how does this change when the intercorrelations of SSTA between ocean basins are accounted for?

To check on this, we performed a multiple linear regression of gridded rainfall anomalies on three SSTA indices: NINO3 (±6°, 90°–150°W), NATL (6°–22°N, 15°–80°W), and SATL (22°S–2°N, 10°E–35°W). The 1979–95 merged (satellite-derived and land rain gauge) rainfall data set of Xie and Arkin (1996) was used for this purpose, and the data at each 2.5- by 2.5-degree square were separately regressed on the predictors. First, however, the monthly data were reduced to annual values. The annual rainy season totals were formed by summing the rainfall for the calendar months in which rainfall exceeded its local climatological median. Within the tropical region of the Americas considered here, the rainy season dates are well defined and uniform over several large contiguous regions. The midseason months are July–August (north of 5°N), March–April (Pacific and Atlantic, 15°S–5°N, and northeastern South America), and December–January (South America south of 5°S). At each grid position the annual rainfall series was correlated with each of the three SSTA indices at both zero lag and for SST leading by 1 year, and the lag for the highest correlation was used in the regression procedure. Predictor terms that did not satisfy an F-test at or above the 95% significance level (serial correlation accounted for) were successively

eliminated in an iterative, backward procedure (Draper and Smith 1966). If two or more predictors are highly intercorrelated, only the one having the strongest relationship with the predictand is likely to survive elimination, regardless of their separate correlations with rainfall.

The percent of rainfall variance explained by the final model is mapped as a measure of overall skill (Fig. 6, upper panel). The final model composition (Fig. 6, lower panel) is mapped into three categories: NINO3 only (lightest shading), Atlantic only (NATL and/or SATL; medium shading), or both basins (NINO3 plus one or two Atlantic predictors; black). For the white areas none of the predictors survived elimination. Explained variance (Fig. 6, upper panel) ranged between 20% and 90%, similarly for all three model categories. A model was successfully extracted over two large contiguous regions, 5°S–20°N, 75°–100°W and 15°S–10°N, 30°–45°W, and less completely over most of northern South America.

The three model categories displayed in Figure 6 differed mainly in the geographical area they cover, not in the ranges of explained variance. As can be seen in the following table of model results, the number of 2-degree grid boxes significant for each predictor varies widely:

Table 1 A compilation of the number of 2-degree grid boxes for which each of the possible regression models is significant, according to the predictors in the surviving model. The NINO3, NATL, and SATL predictors are denoted by N3, NA, and SA, respectively. The "none" category refers to the null model (no significant predictors) indicated by the white squares in Figure 6.

None	N3	NA	SA	N3+NA	N3+SA	NA+SA	N3+NA+SA
146	75	83	51	31	17	28	17

NINO3 is involved in the model over 31% of the spatial domain shown, the North Atlantic over 35%, and the South Atlantic over 25%. The NINO3 predictor completely dominates the rainfall model over and around the NINO3 region (±5° and west of 80°W), but the Atlantic dominates elsewhere and the North Atlantic is the strongest predictor, overall. Poleward of 20°N (not shown), the Atlantic involvement (NATL and SATL) increases to 48% and poleward of 20°S the NINO3 involvement increases to 51% (not shown).

The above analysis does not isolate non-ENSO variability from ENSO, in any of the predictors. Of course, even if all of the partial correlations of Atlantic predictors with rainfall were due to the extended ENSO signal in the Atlantic, one would want to utilize them for prediction because the Atlantic ENSO contributes to the atmospheric response (as explained above from Lau and Nath 1994). However, we note that the NINO3 and NATL correlations are of opposite sign over large areas of Figure 1, which is inconsistent with the positive correlation (+0.5) between the two ocean indices. This result in itself suggests that non-ENSO variability is involved. Another analysis, below, further demonstrates that non-ENSO variability contributes to the relationships.

To see this, we subject the same monthly data sets (SSTA and rainfall anomaly) to an SVD analysis over the domains shown in Figure 7, but for all months of the year (no seasonal stratification). Now, an SVD analysis is essentially a bivariate (two-variable) counterpart to the univariate (one-variable) decomposition frequently referred to as EOF analysis (or PCA). Instead of utilizing and decomposing the covariance structures in a single variable field (such as SSTA alone), it decomposes the cross-covariance structures between two variable fields (in this case, SSTA and rainfall anomaly). Singular value decomposition analysis breaks down into separate modes the ways in which the two variables are spatially (eigenvector maps) and temporally (expansion coefficients) associated with each other. However, for each mode there are two (not one) spatial maps and two sets of temporal expansion coefficients. In this case they correspond to SSTA (upper panel) and rainfall anomaly (lower panel).

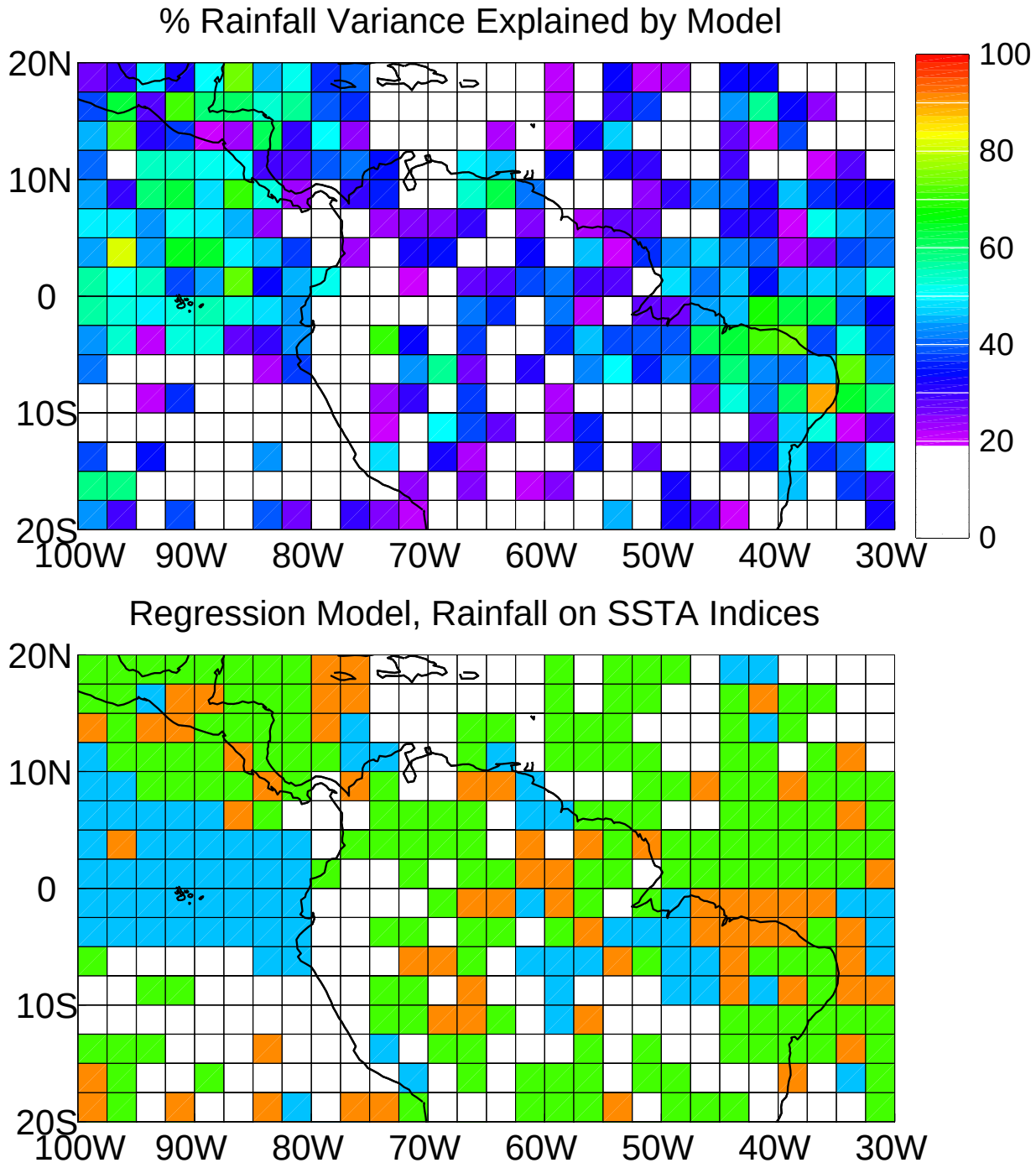

Fig. 6 Results of a multiple linear regression with backward elimination of predictors, of the 2.5- by 2.5-degree gridded rainfall anomalies of Xie and Arkin (1996) on the NINO3, NATL, and SATL indices of sea surface temperature anomalies (SSTA), as described in the text. The upper panel shows the percent variance explained by the final model at each grid location (white is insignificant: <20%). The lower panel describes the model composition as being NINO3 only (blue), Atlantic only (NATL and/or SATL; green), or both oceans (NINO3 plus NATL and/or SATL; orange).

The covariability of SSTA and rainfall anomaly associated with ENSO emerge in the first mode (not shown), which accounts for 72% of the squared cross-covariance. In terms of SSTA, this mode is virtually identical to what we think of as ENSO, with a correlation of 0.97 between the SSTA expansion coefficients and the NINO3 time series. In this mode, a strongly warm equatorial Pacific (El Niño) combines with a moderately warm tropical North Atlantic and cool tropical South Atlantic to produce a rainfall pattern that corresponds qualitatively to ENSO-related features already recognized from other studies (e.g., Ropelewski and Halpert 1987, 1989). The next three modes correspond to covariability between SSTA and rainfall that is unaccounted for by the first (ENSO) mode. They account for 16% of the squared cross-covariance, but correlate significantly only with NATL and/or SATL. In the second mode (Fig. 7) the correlation of the SSTA expansion coefficients with NATL is 0.58, and the correlation with NATL-SATL (dipole) is 0.69.

Figure 7 shows that a strongly warm tropical North Atlantic combines with a moderately cool tropical Pacific and South Atlantic to produce positive departures of rainfall over Central America and the Caribbean as well as in the range of the eastern Pacific ITCZ. Under such circumstances, the vector correlations of the surface wind anomalies from the Comprehensive Ocean-Atmosphere Data Set (COADS; Woodruff et al. 1987) with the second mode expansion coefficients for SSTA (upper panel) show that the northeast trades are weakened over this region and over the tropical North Atlantic. This weakening is consistent with the analysis of Enfield and Mayer (1997), wherein reductions in the strength of the North Atlantic trade winds lead to warmings of the tropical North Atlantic.

The vector correlations of the wind anomalies with the temporal expansion coefficients for the rainfall side of the SVD mode are shown in the lower panel of Figure 7. They show that strong fluctuations in the easterly winds occur in the same area as the strong rainfall response, in the range of the ITCZ. In other words, a cool eastern Pacific, when combined with a strong positive dipole in the Atlantic, is associated with excess rainfall and reduced easterly wind flow over the Caribbean, Central America, and the eastern Pacific ITCZ. In that region, the rainfall response (i.e., the explained covariability between SSTA and rainfall) is much stronger than in the ENSO mode. The enhanced rainfall is consistent with greater tropospheric instability and convection and with greater low-level wind convergence within the ITCZ. The sense of the wind correlations suggests an accentuation of the southwest monsoonal flow south of the ITCZ that is normally associated with enhanced convection and rainfall during the boreal summer.

It is noteworthy that the sense of the Pacific SSTA in mode 2 is reversed with respect to that of the Atlantic dipole, as contrasted to the first (ENSO) mode, where the equatorial Pacific and the tropical North Atlantic SSTA have the same sign. In the third and fourth modes (not shown), the tropical Atlantic assumes a monopole configuration and combines with a cool or warm Pacific, respectively. We attribute no unique physical significance to any of the higher modes (2, 3, 4). However, these modes tell us that non-ENSO SST variability in the Atlantic combines in various ways with variability in the Pacific to explain a sizable fraction (0.16) of the squared cross-covariance between the SSTA and rainfall data sets. We can also see that when the east Pacific and tropical North Atlantic SSTAs are oppositely signed, the anomalous rainfall response over the Caribbean and most of Central America is enhanced. Further research will be required to find out why this is so.

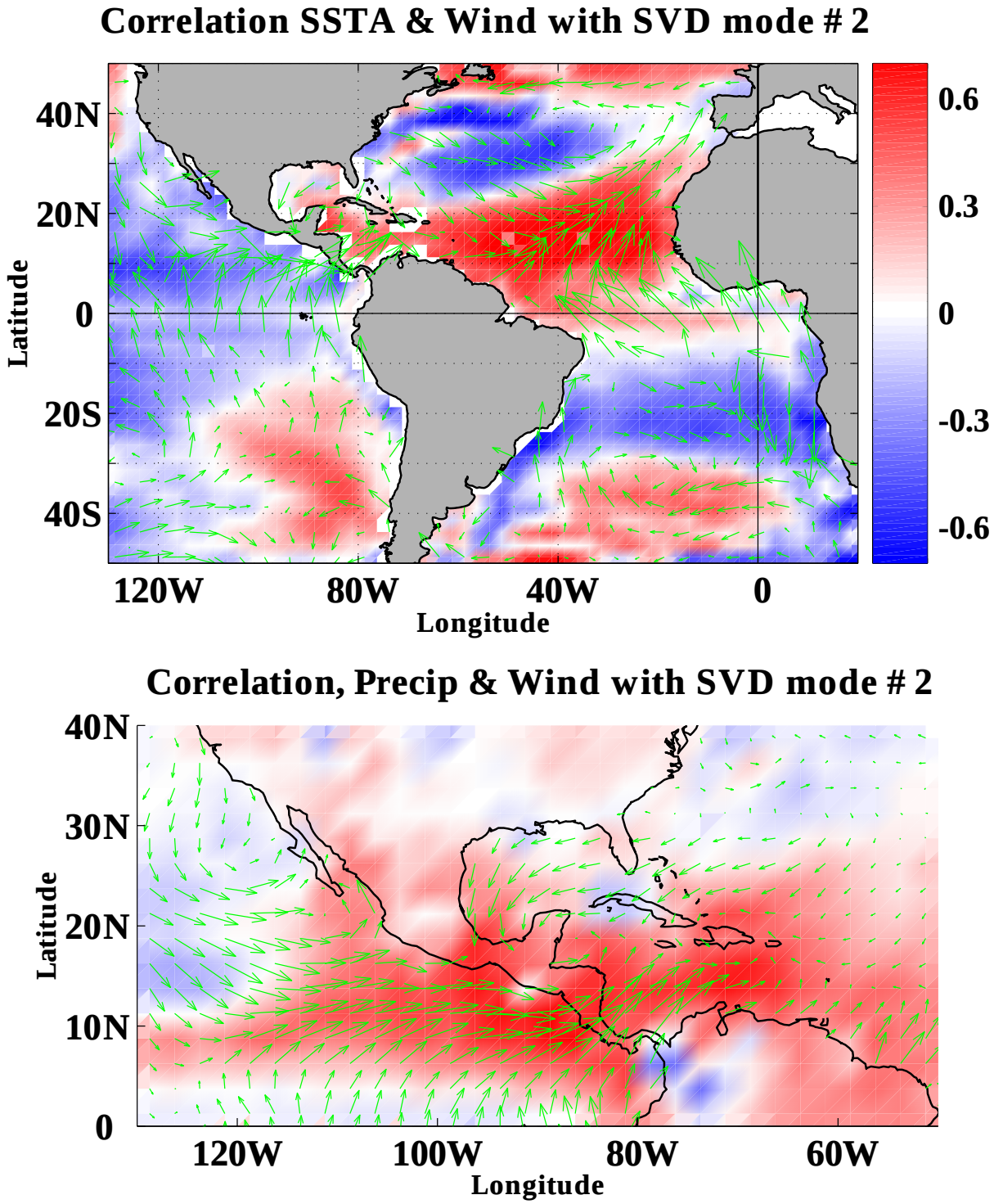

Fig. 7: Second mode of a singular vector decomposition (SVD) analysis of sea surface temperature anomalies (SSTA) and Xie and Arkin (1996) rainfall anomaly over the spatial domains shown in the upper and lower panels, respectively. The upper panel shows the homogeneous correlation map for gridded SSTA vs. the temporal expansion coefficients for SSTA (colored shading). The lower panel shows the homogeneous correlation map for rainfall vs. the temporal expansion coefficients for rainfall (colored shading). Arrows are the vector correlations for the gridded Comprehensive Ocean Atmosphere Data Set (COADS) surface wind anomalies vs. the respective expansion coefficients.

There is an unresolved question of seasonality in the relationships described here, because the SVD analysis was performed for all months of the year. However, the first mode is overwhelmingly dominated by the ENSO-related SSTA variability in the Pacific cold tongue (NINO3). Since every peak (positive or negative) in the NINO3 time series occurs in the November-December-January period, we can safely infer that the mode 1 rainfall relationships correspond to the boreal winter. The consistency of mode 1 with the results of Ropelewski and Halpert (1987) supports this inference. Because the large rainfall response in mode 2 occurs in a region where a sharp dichotomy exists between the very dry months of the boreal winter and the much wetter months of the summer, it is most likely a summer phenomenon (May through November).

Conclusions

In this chapter we have combined new analyses of SST and rainfall data, together with a review of previous work by others, to underline several important points:

(1) ENSO-related SST variability is strongest in the Pacific Ocean but extends to the tropical Atlantic and Indian Oceans as well, with systematic lags of 1 to 3 seasons consistent with tropospheric forcing between basins.

(2) After a global ENSO mode is properly removed from the SST data, the residual variability emerges in three additional modes that correspond to phenomena previously identified by others: (a) a mode dominated by global warming; (b) an interdecadal Pacific mode with strong loading in the extratropical North Pacific; and (c) a multidecadal mode with its greatest intensity in the extratropical North Atlantic.

(3) El Niño/Southern Oscillation variability in the other ocean basins is not redundant in regard to associated atmospheric responses.

(4) In the western hemisphere tropics, both the Atlantic and the Pacific covary with rainfall in significant and unique ways; although the global ENSO is the dominant process, non-ENSO variability provides a sizable increase in the explained cross-covariance between SSTA and rainfall.

While ENSO is clearly the dominant process, the non-ENSO variability that emerges from the CEOF analysis (Figs. 3, 4, and 5) is fairly robust, and the non-ENSO modes can be easily related in myriad ways to analyses previously done by others. Our conclusions (3) and (4) apply strictly to ENSO and non-ENSO fluctuations in the tropics, where the SSTA variability is dominated by the relatively short, interannual to decadal time scales. It is likely that the same principles can be extended to the non-ENSO modes of variability that dominate at higher latitudes and on longer time scales. Predictions of climate several months to several seasons ahead can be improved by also projecting the tendencies of the non-ENSO modes which form the slowly varying background to the interannual variability. Both the ENSO and the non-ENSO processes should be considered globally, and coupled models (with global model oceans) should be made to emulate them.

Acknowledgements

We wish to thank T. Smith, A. Kaplan, and P. Xie for making their SST and rainfall data sets public and helping us obtain them. We also credit useful exchanges with H. Diaz, R. Houghton, M. Latif, D. Mayer, and Y. Tourre for contributing to our enlightenment. Our research has been supported by the National Oceanic and Atmospheric Administration (NOAA) through its Pan-American Climate Studies program, by the Inter-American Institute for Global Change Research (IAI), and by the NOAA Environmental Research Laboratories through their base funding of our laboratory.

References

Barnston, A.G., and Livezey, R.E., 1987: Classification, seasonality and persistence of low-frequency atmospheric circulation patterns. *Monthly Weather Review*, **115**, 1083–1126.

Barnston, A., Van den Dool, H.M., Zebiak, S.E., Barnett, T.P., Ji, M., Rodenhuis, D.R,. Cane, M.A., Leetmaa, A., Graham, N.E., Ropelewski, C.R., Kousky, V.E., O'Lenic, E.A., and Livezey, R.E., 1994: Long-lead seasonal forecasts—where do we stand? *Bulletin of the American Meteorological Society*, **75**, 2097–2114.

Cane, M.A., Clement, A.C., Kaplan, A., Kushnir, Y., Pozdnyakov, D., Seager, R., Zebiak, S.E., and Murtugudde, R., 1997: Twentieth-century sea surface temperature trends. *Science*, **275**, 957–960.

Carton, J., and Huang, B., 1994: Warm events in the tropical Atlantic. *Journal of Physical Oceanography*, **24,** 888–903.

Chang, P., Ji, L., and Li, H., 1997: A decadal climate variation in the tropical Atlantic Ocean from thermodynamic air-sea interactions. *Nature*, **385**, 516–518.

Citeau, J., Finaud, L., Cammas, J.P., and Demarcq, H., 1989: Questions relative to ITCZ migrations over the tropical Atlantic Ocean, sea surface temperature and Senegal River runoff. *Meteorology & Atmospheric Physics*, **41**, 181–190.

Covey, D.C., and Hastenrath, S., 1978: The Pacific El Niño phenomenon and the Atlantic circulation. *Monthly Weather Review*, **106**, 1280–1287.

Curry, R.G., and McCartney, M.S., 1996: North Atlantic's transformation pipeline. *Oceanus*, **39**, 24–28.

Delworth, T.L., 1996: North Atlantic interannual variability in a coupled ocean-atmosphere model. *Journal of Climate*, **9,** 2356–2375.

Deser, C., and Blackmon, M.L., 1993: Surface climate variations over the North Atlantic Ocean during winter: 1900–1989. *Journal of Climate*, **6**, 1743–1753.

Deser, C., and Blackmon, M.L., 1995: On the relationship between tropical and North Pacific sea surface temperature variations. *Journal of Climate*, **8**, 1677–1680.

Draper, N., and Smith, H., 1966: *Applied Regression Analysis*. New York: Wiley and Sons, 709 pp.

Enfield, D.B., 1989: El Niño, past and present. *Reviews of Geophysics*, **27**, 159–187.

Enfield, D.B., 1996: Relationships of inter-American rainfall to tropical Atlantic and Pacific SST variability. *Geophysical Research Letters*, **23**, 3505–3508.

Enfield, D.B., and Mayer, D.A., 1997: Tropical Atlantic SST variability and its relation to El Niño-Southern Oscillation. *Journal of Geophysical Research*, **102,** 929–945.

Folland, C.K., Palmer, T.N., and Parker, D.E., 1986: Sahel rainfall and worldwide sea temperatures. *Nature,* **320**, 602–607.

Gu, D., and Philander, S.G.H., 1997: Interdecadal climate fluctuations that depend on exchanges between the tropics and extratropics. *Science,* **275**, 721–892.

Hameed, S., Sperber, K.R., and Meinster, A., 1993: Teleconnections of the Southern Oscillation in the tropical Atlantic sector in the OSU coupled upper ocean-atmosphere GCM. *Journal of Climate*, **6**, 487–498.

Hansen, D.V., and Bezdek, H.F., 1996: On the nature of decadal anomalies in North Atlantic sea surface temperature. *Journal of Geophysical Research,* **101**, 8749–8758.

Hastenrath, S., 1978: On modes of tropical circulation and climate anomalies. *Journal of the Atmospheric Sciences,* **35**, 2222–2231.

Hastenrath, S., 1984: Interannual variability and the annual cycle: Mechanisms of circulation and climate in the tropical Atlantic sector. *Monthly Weather Review,* **112**, 1097–1107.

Hastenrath, S., de Castro, L.C., and Aceituno, P., 1987: The Southern Oscillation in the Atlantic sector. *Contributions in Atmospheric Physics*, **60**, 447–463.

Hastenrath, S., and Greischar, L., 1993: Further work on the prediction of northeast Brazil rainfall anomalies. *Journal of Climate*, **6**, 743–758.

Houghton, J.T., Meira Filho, L.G., Callander, B.A., Harris, N., Kattenberg, A., and Maskell, K. (eds.), 1996: *Climate Change 1995, the Science of Climate Change.* Cambridge: Cambridge University Press, 572 pp.

Houghton, R.W., and Tourre, Y.M., 1992: Characteristics of low-frequency sea surface temperature fluctuations in the tropical Atlantic. *Journal of Climate,* **5**, 765–771.

Huang, B., Carton, J.A., and Shukla, J., 1995: A numerical simulation of the variability in the tropical Atlantic Ocean, 1980–88. *Journal of Physical Oceanography,* **25**, 836–854.

Hurrell, J.W., 1995: Decadal trends in the North Atlantic Oscillation: Regional temperatures and precipitation. *Science,* **269**, 676–679.

Jones, P.D., Bradley, R.S., Diaz, H.F., Kelley, P.M., and Wigley, T.M.L., 1986: Northern hemisphere surface air temperature variations: 1851–1984. *Journal of Climate and Applied Meteorology*, **25**, 161–179.

Kaplan, A., Cane, M.A., Kushnir, Y., Clement, A.C., Blumenthal, M.B., and Rajagopalan, B., 1998: Analysis of Global Sea Surface Temperatures 1856-1991, *Journal of Geophysical Research*, in press.

Kawamura, R., 1994: A rotated analysis of global sea surface temperature variability with interannual and interdecadal scales. *Journal of Physical Oceanography*, **24**, 707–715.

Kerr, R.A., 1997: A new driver for the Atlantic's moods and Europe's weather? *Science,* **275**, 754–755.

Kushnir, Y., 1994: Interdecadal variations in North Atlantic sea surface temperature and associated atmospheric conditions. *Journal of Climate,* **7**, 141–157.

Lamb, P.J., and Peppler, R.A., 1992: Further case studies of tropical Atlantic surface atmospheric and oceanic patterns associated with sub-Saharan drought. *Journal of Climate*, **5**, 476–488.

Lanzante, J.L., 1996: Lag relationships involving tropical sea surface temperatures. *Journal of Physical Oceanography,* **9**, 2568–2578.

Latif, M., and Barnett, T.P., 1994: Causes of decadal climate variability over the North Pacific and North America. *Science,* **266**, 634–637.

Latif, M., and Barnett, T. P., 1995: Interactions of the tropical oceans. *Journal of Climate*, **8**, 952–964.

Latif, M., and Barnett, T.P., 1996: Decadal climate variability over the North Pacific and North America: Dynamics and predictability. *Journal of Climate*, **9**, 2407–2423.

Lau, N.C., and Nath, M.J., 1994: A modeling study of the relative roles of tropical and extratropical anomalies in the variability of the global atmosphere-ocean system. *Journal of Climate*, **7**, 1184–1207.

McCartney, M.S., Curry, R.G., and Bezdek, H.F., 1996: North Atlantic's transformation pipeline chills and redistributes subtropical water. *Oceanus,* **39**, 19–23.

Mehta, V.M., and Delworth, T., 1995: Decadal variability of the tropical Atlantic Ocean surface temperature in shipboard measurements and in a global ocean-atmosphere model. *Journal of Climate*, **8**, 172–190.

Moura, A.D., and Shukla, J., 1981: On the dynamics of droughts in northeast Brazil: Observations, theory and numerical experiments with a general circulation model. *Journal of the Atmospheric Sciences,* **38**, 2653–2675.

Nicholls, N., Lavery, B., Frederiksen, C., and Drosdowsky, W., 1996: Recent apparent changes in relationships between the El Niño-Southern Oscillation and Australian rainfall and temperature. *Geophysical Research Letters,* **23**, 3357–3360.

Nobre, P., and Shukla, J., 1996: Variations of sea surface temperature, wind stress, and rainfall over the tropical Atlantic and South America. *Journal of Climate,* **9**, 2464–2479.

Philander, S.G.H., 1990: *El Niño, La Niña and the Southern Oscillation*. New York: Academic Press, 293 pp.

Rasmusson, E.M., and Carpenter, T.C., 1982: Variations in tropical sea surface temperature and surface wind fields associated with the Southern Oscillation/El Niño. *Monthly Weather Review,* **110**, 354–384.

Rasmusson, E.M., Arkin, P.A., Chen, W.Y., and Jallickee, J.B., 1981: Biennial variations in surface temperature over the United States as revealed by singular decomposition. *Monthly Weather Review,* **109**, 588–598.

Ropelewski, C.F., and Halpert, M.S., 1987: Global and regional scale precipitation patterns associated with the El Niño-Southern Oscillation. *Monthly Weather Review,* **110**, 1606–1626.

Ropelewski, C.F., and Halpert, M.S., 1989: Precipitation patterns associated with the high index phase of the Southern Oscillation. *Journal of Climate,* **2**, 268–284.

Servain, J., 1991: Simple climatic indices for the tropical Atlantic Ocean and some applications. *Journal of Geophysical Research,* **96**, 15137–15146.

Smith, T.M., Reynolds, R.W., Livezey, R.E., and Stokes, D.C., 1996: Reconstruction of historical sea surface temperatures using empirical orthogonal functions. *Journal of Climate,* **9**, 1403–1420.

Ting, M., and Wang, H., 1997: Summertime United States precipitation variability and its relation to Pacific sea surface temperature. *Journal of Climate,* **10**, 1853–1873.

Tourre, Y.M., and White, W.B., 1995: ENSO signals in global upper-ocean temperature. *Journal of Physical Oceanography*, **25**, 1317–1332.

Trenberth, K.E., and Hurrell, J.W., 1994: Decadal atmosphere-ocean variations in the Pacific. *Climate Dynamics,* **9**, 303–319.

Wagner, R.G., 1996: Mechanisms controlling variability of the interhemispheric sea surface temperature gradient in the tropical Atlantic. *Journal of Climate,* **9**, 2010–2019.

Wallace, J.M., Smith, C., and Jiang, Q., 1990: Spatial patterns of atmosphere-ocean interaction in northern winter. *Journal of Climate,* **3**, 990–998.

Weare, B.C., 1977: Empirical orthogonal function analysis of Atlantic Ocean surface temperatures. *Quarterly Journal of the Royal Meteorological Society*, **103**, 467–478.

Woodruff, S.D., Slutz, R.J., Jenne, R.L., and Steurer, P.M., 1987: A comprehensive ocean-atmosphere data set. *Bulletin of the American Meteorological Society*, **68**, 1239–2278.

Xie, P., and Arkin, P.A., 1996: Analyses of global monthly precipitation using gauge observations, satellite estimates, and numerical model predictions. *Journal of Climate*, **9**, 840–858.